Proceedings of the 9th International Symposium on
Dynamics and Control of Process Systems (DYCOPS 2010),
Leuven, Belgium, July 5-7, 2010
Mayuresh Kothare, Moses Tade, Alain Vande Wouwer, Ilse Smets (Eds.)

Modelling of Detailed Insulin Receptor Kinetics Affects Sensitivity and Noise in the Downstream Signalling Pathway ⋆

Camilla Luni * **Kevin R. Sanft** ** **Linda R. Petzold** ***
Francis J. Doyle III ****

* *Chemical Engineering Department, University of California at Santa Barbara, Santa Barbara, CA 93106-5080 USA (e-mail: lunicam@engineering.ucsb.edu)*
** *Computer Science Department, University of California at Santa Barbara, Santa Barbara, CA 93106-5070 USA (e-mail: sanftk@cs.ucsb.edu)*
*** *Computer Science Department, University of California at Santa Barbara, Santa Barbara, CA 93106-5070 USA (e-mail: petzold@cs.ucsb.edu)*
**** *Chemical Engineering Department, University of California at Santa Barbara, Santa Barbara, CA 93106-5080 USA (e-mail: frank.doyle@icb.ucsb.edu)*

Abstract: Insulin resistance is a primary defect underlying the development of type II diabetes. In healthy conditions, insulin stimulates glucose uptake from the blood stream, but in diseased conditions the normal metabolic response is impaired. Identifying specific drug targets to restore insulin sensitivity at the cellular level and developing an effective treatment strategy require insight into both the biochemical mechanisms involved and the whole signalling network response to external cues. This study focuses on the consequences of integrating a detailed biochemical description of the insulin receptor trafficking compartment within a phenomenological model of the downstream signalling pathway. While the description of the experimental data is preserved by an iterative procedure of parameter fitting, the dynamic response of the network is highly modified, as shown by analyzing the complementary information derived from studying both connection sensitivities and node noise in the network. This is crucial considering the importance of network dynamics for identifying effective drug targets.

Keywords: Insulin, diabetes, signalling pathway, sensitivity analysis, drug target, stochastic modelling.

1. INTRODUCTION

Type II diabetes mellitus is a metabolic disease involving dysfunction in the regulation of glucose homeostasis. It has a complex pathology involving both genetic predisposition and environmental factors, related to sedentary lifestyle and obesity (Leahi [2005]).

A primary defect underlying the development of this disease is insulin resistance. While in healthy conditions insulin stimulates glucose uptake from the blood stream, in disease conditions the normal metabolic response is impaired (Defronzo et al. [1991]). Adipose tissue, together with skeletal muscle, play a crucial role in glucose homeostasis. Adipocytes normally bind insulin to their membrane receptors that trigger an intracellular signalling cascade that ultimately stimulates glucose transporter GLUT4 translocation to the cell membrane, allowing glucose entrance into the cell (Rosen and Spiegelman [2006]).

Identifying specific drug targets, for example, to restore insulin sensitivity at the cellular level, and developing an effective treatment strategy require insight not only on the whole signalling network response to external cues, but also on the biochemical mechanisms involved (Schrattenholz and Soskić [2008]). Protein structures and protein-protein interactions play a major role in drug discovery, and structural models are developed hand in hand with the experimental techniques that make possible the validation of their predictions (Edwards [2009]).

A detailed description of insulin receptor dynamics has been presented by Kiselyov et al. [2009]. They developed a physically plausible model of the receptor activation starting from the available structural information, and verified its thermodynamic consistency.

⋆ This work was funded by Pfizer Inc. K.S. and L.P. were also supported by Grant No. R01EB007511 from the National Institute of Biomedical Imaging and Bioengineering, DOE Contract No. DE-FG02-04ER25621, NSF Contract No. IGERT DG02-21715, and the Institute for Collaborative Biotechnologies through Grant No. DFR3A-8-447850-23002 from the U.S. Army Research Office. K.S. was supported by a National Science Foundation Graduate Research Fellowship.

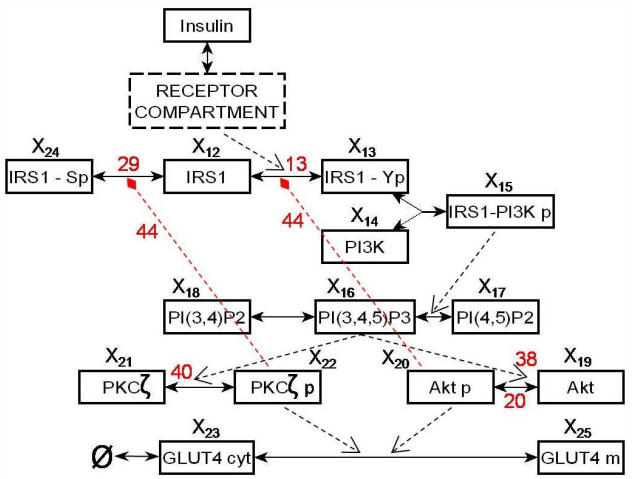

Fig. 1. Schematic of the insulin signalling pathway model. Symbols and $X_{i,i\in[1,25]}$ are explained in Appendix A. Solid arrows represent chemical reactions, black dashed arrows activation, and red dashed arrows two negative regulatory feedbacks. $\emptyset$ represents GLUT4 production/degradation. Red numbers are the parameters that particularly affect GLUT4m, as shown in Fig. 4.

In this work, we focus on the implications of incorporating the detailed biochemical description of the insulin receptor trafficking compartment (Kiselyov et al. [2009]) within a phenomenological model of the downstream signalling pathway (Sedaghat et al. [2002]). Integrating these aspects into a multiscale model allowed in silico simulations to identify critical kinetic parameter sensitivities and stochastic effect propagation.

2. MODEL

The most detailed currently available model of insulin signalling pathway was developed by Sedaghat et al. [2002]. It accounts for the main known processes involved between insulin stimulation and GLUT4 translocation to the cell membrane, whose schematic is shown in Fig. 1. Briefly, insulin receptor undergoes autophosphorylation and activation after insulin binding. Then, it tyrosine phosphorylates insulin receptor substrate-1 (IRS1), which in turn serves as a docking site for phosphatidylinositide 3-kinase (PI3K). IRS1 can also be serine phosphorylated. The complex IRS1-PI3K catalyzes the production of phosphatidylinositol 3,4,5-triphosphate (PI(3,4,5)P3) from phosphatidylinositol 4,5-bisphosphate (PI(4,5)P2). PI(3,4,5)P3 can also be dephosphorylated to phosphatidylinositol 3,4-bisphosphate (PI(3,4)P2). Activation, through phosphorylation, of downstream kinases Akt and PKCζ is dependent on the concentration level of PI(3,4,5)P3. GLUT4 is produced and degraded within the intracellular compartment, and is translocated to the cell membrane at a rate that is indirectly dependent on the level of phosphorylated Akt and PKCζ. Two feedback loops further complicate the signalling cascade: phosphorylated Akt inhibits IRS1 tyrosine dephosphorylation, while phosphorylated PKCζ inhibits IRS1 serine dephosphorylation. This model is considered as a basis for comparison in the following discussion.

We modified Sedaghat's model, building a multiscale model that accounts for detailed biochemical insulin-receptor interactions within the receptor compartment (Kiselyov et al. [2009]). Fig. 2 shows the network of reactions included. With respect to the model proposed by Kiselyov et al. [2009], the number of components in the network was reduced by considering symmetric insulin-receptor complexes as the same components in the network. Details on the equations for the receptor compartment are provided in Appendix B. For equations downstream in the pathway the interested reader is referred to Sedaghat et al. [2002].

The parameters of the multiscale model were fitted to the experimental data presented in Sedaghat et al. [2002], and a list of parameter values is reported in Appendix C. All computational simulations were performed using MATLAB (The MathWorks, Inc.).

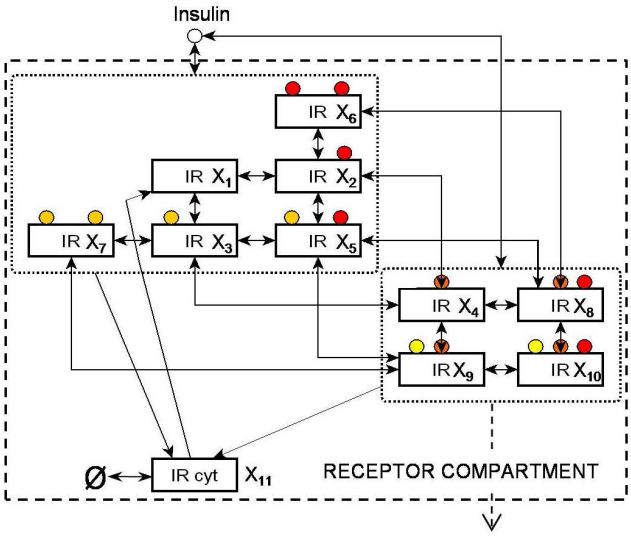

Fig. 2. Detailed schematic of the insulin receptor (IR) compartment. Circles indicate insulin molecules. Yellow and red circles represent insulin molecules attached to either of two binding sites; orange circles are those attached to both sites. IR cyt is the intracellular insulin receptor. Solid arrows represent chemical reactions, the dashed arrow downstream activation. The upper left dotted box includes inactive forms of the receptor, the lower right contains the active ones.

Fig. 3 shows an example of the temporal profiles obtained by the two models. Free insulin receptor concentration is in perfect agreement between the two models, and the biphasic response of PKCζ, reported in the experimental work by Standaert et al. [1999], is also reproduced. In general, the description of the experimental data is preserved by the iterative procedure of parameter fitting.

3. SENSITIVITY ANALISYS

3.1 Methods

To determine if the parameters have an altered impact on the system's behaviour, a local sensitivity analysis (Saltelli et al. [2000]) was performed for both Sedaghat's and our multiscale model. The sensitivity coefficients, S_i, were normalized as follows:

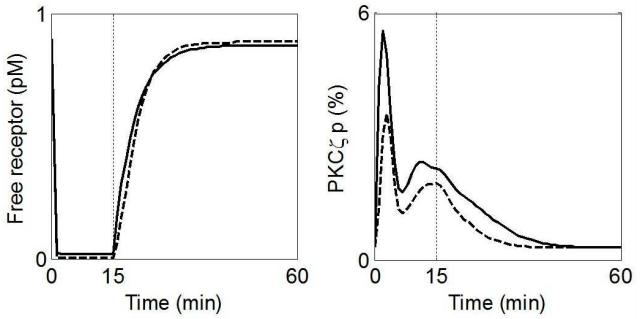

Fig. 3. Temporal profiles of free insulin receptor (A), and activated PKCζ (B), in response to a step of 100-nM insulin, which is removed after 15 minutes. The dashed line represents results from the multiscale model; the solid line gives the results from Sedaghat et al. [2002].

$$S_i = \frac{\partial [GLUT4m]}{\partial k_i} \cdot \frac{k_i}{[GLUT4m]} \tag{1}$$

where k_i represents the generic model parameter and $[GLUT4m]$ indicates membrane GLUT4 concentration. GLUT4m was the chosen output as it is the actual glucose transporter into the cell, and thus directly correlated with the ability of the cell to uptake glucose. The mean sensitivity coefficients, $\bar{S}_i$, over a 15-minute step of 100 nM insulin stimulation were calculated as in:

$$\bar{S}_i = {t_f}^{-1} \cdot \int_0^{t_f} S_i dt \tag{2}$$

where t_f = 15min. Fig. 4 shows the results for the parameters common to both models, in terms of the difference between the absolute values of in the multiscale and in Sedaghat's model.

3.2 Results and Analysis

The results of the sensitivity analysis (Fig. 4) show significant differences even though the parameters are involved in parts of the network that are downstream from the receptor compartment and modelled in the same way in both models (the parameter numbers are highlighted in red in Fig. 1). Specifically, in the multiscale model, GLUT4m has an increased sensitivity to parameters describing IRS1 tyrosine and serine phosphorylation, and PKCζ tyrosine phosphorylation. A decreased sensitivity is shown to the parameters involved in both Akt phosphorylation and dephosphorylation. Interestingly, phosphorylated Akt resulted also in significantly less noise in stochastic simulations, as discussed below. Furthermore, in the multiscale model parameter 44, involved in the two feedback loops, is less sensitive.

Since parameter sensitivity is often used to identify which parameters in the model should be determined more precisely via expensive biological experiments, the insights gained by using a detailed network description are potentially very valuable. For example, we discovered that parameters related to the Akt node are less sensitive than previously found using the model by Sedaghat et al. [2002].

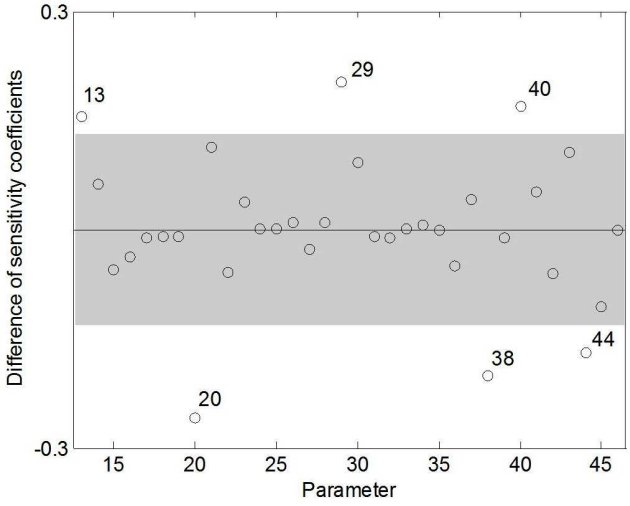

Fig. 4. Results from local sensitivity analysis. Each circle represents the difference between the absolute value of $\bar{S}_i$ of the multiscale model and Sedaghat et al. [2002] with respect to the parameter indicated. The shaded area represents the region where the difference between the two models is negligible, assuming a threshold of 0.12, i.e. the difference is less than 12%.

Fig. 5 shows the temporal profiles of the sensitivity coefficients that showed more remarkable differences between the two models (Fig. 4). The simulation included a 100nM insulin pulse for 15 minutes followed by 45 minutes without insulin.

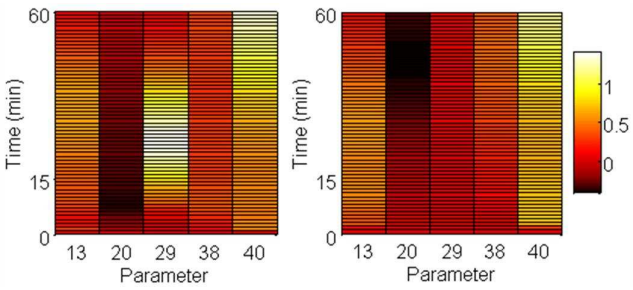

Fig. 5. Temporal profiles of the normalized sensitivity coefficients for Sedaghat's model (left) and the multiscale model (right). The output considered is GLUT4m. The simulation includes 15 minutes at 100nM insulin concentration, and 45 minutes at 0 concentration.

Parameter 20 in Sedaghat's model is more identifiable after insulin removal than during the pulse, the contrary being true for the multiscale model (Fig. 5). Thus, these results underscore the importance of experimental approaches that design input dynamics to maximize parameter identifiability (Kwei et al. [2008]).

4. STOCHASTIC SIMULATIONS

4.1 Methods

Previous work has demonstrated substantial intrinsic fluctuations in a stochastic adaptation of Sedaghat's model (Kwei et al. [2008]). To investigate the impact of incorporating detailed receptor dynamics on stochastic noise, we

constructed a stochastic version of the multiscale model. For details on the conversion of the two deterministic models into stochastic form, the reader is referred to Kwei et al. [2008].

An ensemble of 1000 stochastic simulations of both models was run to get estimates of the mean and standard deviation of all state variables at several time points. The coefficient of variation (CV = standard deviation/mean) was calculated and used as the measure of noise to make results comparable between the different variables. The mean coefficients of variation, $\overline{CV}_i$, over a 15-minute step of 100nM insulin stimulation were calculated as in:

$$\overline{CV}_i = {t_f}^{-1} \cdot \int_0^{t_f} CV_i \, dt \tag{3}$$

where index i refers to the different components in the network.

4.2 Results and Analysis

The stochastic counterparts of the two deterministic models highlighted differences in the way noise propagates through the network. When stimulated with a 100nM insulin pulse input for 15 minutes, the output from the receptor compartment, $(X_4 + X_8 + X_9 + X_{10})$ for the multiscale model, was noisier than in Sedaghat's model with a $\overline{CV} \approx 5.6\%$ compared to $\overline{CV} \approx 1\%$. This led to significant modification of noise in several downstream component concentrations (Fig. 6), due in part to the effects of the two feedback loops present in the cascade. One component, phosphorylated Akt, resulted in significantly less noise, as shown in Fig. 6.

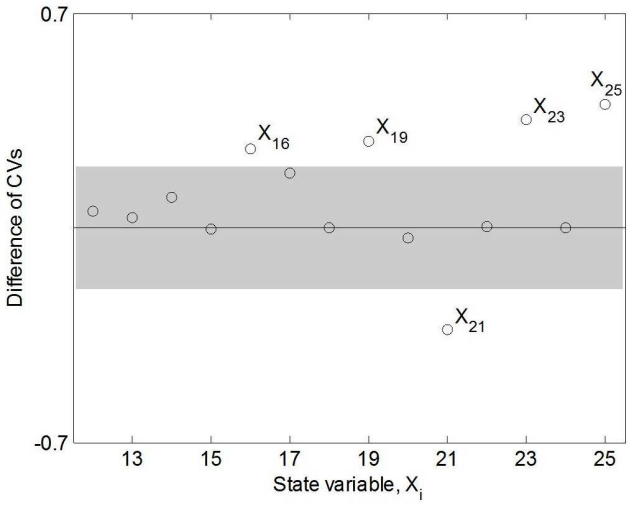

Fig. 6. Results from stochastic simulations. Each circle represents the difference between $\overline{CV}$ of the multiscale model and Sedaghat et al. [2002] with respect to the state variable indicated. The shaded area represents the region where the difference between the two models is negligible, assuming a threshold of 0.2, i.e. the difference is less than 20%.

The differences in stochastic noise that can arise by incorporating biochemical details into a network model can have important implications for drug targeting. If the impact on stochastic fluctuations is not well understood, an otherwise effective intervention could lead to excessive fluctuations in the network that trigger unexpected side effects.

5. DISCUSSION AND CONCLUSION

The development of drugs to pinpoint specific molecular targets requires knowledge of the biochemical interactions between the components involved. Due to the highly complex and interactive character of intracellular regulatory networks, biochemical interactions should be considered within this context (Kitano [2002], Barabási and Oltvai [2004]). On the other hand, computational simulations of network behaviour show that network response is also affected by the introduction of detailed biochemical mechanisms.

As an example, in this work we integrated a detailed model of insulin-receptor interaction into a phenomenological description of the signalling cascade that triggers GLUT4 translocation to the cell membrane promoting glucose uptake. We showed how parametric sensitivities and stochastic noise in the concentrations in the downstream network compartment were subsequently modified, despite the fact that parameters were adjusted to fit the same experimental data.

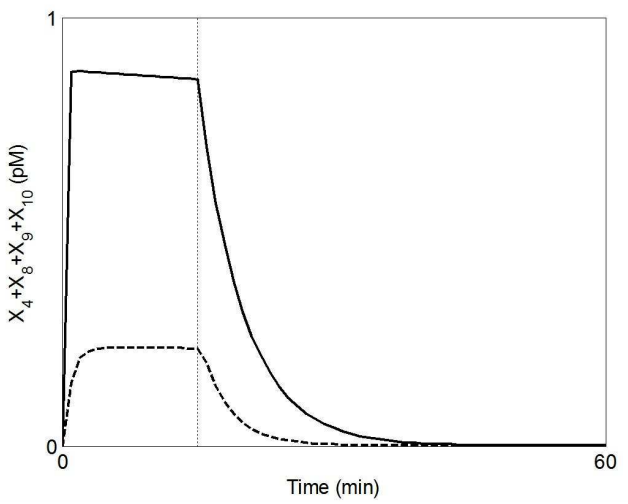

Fig. 7. Temporal profiles of the activated insulin receptor in response to a step of 100-nM insulin, which is removed after 15 minutes. The dashed line represents results from the multiscale model; the solid line gives the results from Sedaghat et al. [2002].

The main consequence of inserting biochemical details into the original model is the modification of the temporal profile of the output from the receptor compartment, $(X_4 + X_8 + X_9 + X_{10})$ for the multiscale model, shown in Fig. 7. The experimental data are well described by both models (Fig. 3). Nonetheless, they do not constrain the profiles in Fig. 7 that have similar qualitative behaviours, but are significantly different in the magnitudes of the maximum concentration reached. This produces the differences, analyzed above in terms of sensitivity coefficients and stochastic noise, in the downstream compartment.

We pointed out how biochemical details affect network behaviour analyzing the complementary information derived by studying both connection sensitivities and node noise in the network. The behaviour of the whole network model is highly modified when a compartment is replaced by an expanded one including more detailed biochemical interactions, unless the experimental data precisely constrain the connections of this module with the remaining network.

REFERENCES

Barabási, A., and Oltvai, Z.N. (2004). Network biology: understanding the cell's functional organization. *Nature Reviews Genetics*, 5:101–113.

Defronzo, R.A. and Ferrannini, E. (1991). Insulin resistance - a multifaceted syndrome responsible for NIDDM, obesity, hypertension, dyslipidemia, and atherosclerotic cardiovascular disease. *Diabetes Care*, 14(3):173–194.

Edwards, A. (2009). Large-scale structural biology of the human proteome. *Annual Review of Biochemistry*, 78: 541–568.

Kiselyov, V.V., Versteyhe, S., Gauguin, L., and De Meyts, P. (2009). Harmonic oscillator model of the insulin and IGF1 receptors' allosteric binding and activation. *Molecular Systems Biology*, 5 (243), Epub 2009 Feb 17.

Kitano, H. (2002). Computational systems biology. *Nature*, 420, 206-210.

Kwei, E.C., Sanft, K.R., Petzold, L.R., and Doyle III, F.J. (2008). Systems analysis of the insulin signaling pathway. *Proceedings of the 17th IFAC World Congress*, 17(1). 10.3182/20080706-5-KR-1001.3822.

Leahi, J.L. (2005). Pathogenesis of Type 2 Diabetes Mellitus. *Archives of Medical Research*, 36 (3), 197-209.

Rosen, E.D. and Spiegelman, B.M. (2006). Adipocytes as regulators of energy balance and glucose homeostasis. *Nature*, 444 (7121), 847-853.

Saltelli, A., Chan, K., and Scott, E.M. (2000). *Sensitivity analysis*. John Wiley & Sons Ltd, England.

Schrattenholz, A. and Soskić, V. (2008). What does systems biology mean for drug development? *Current Medicinal Chemistry*, 15 (15), 1520-1528.

Sedaghat, A.R., Sherman, A., and Quon, M.J. (2002). A mathematical model of metabolic insulin signaling pathways. American *Journal of Physiology - Endocrinology and Metabolism*, 283 (5), E1084-E1101.

Standaert, M.L., Bandyopadhyay, G., Perez, L., Price, D., Galloway, L., Poklepovic, A., Sajan, M.P., Cenni, V., Sirri, A., Moscat, J., Toker, A., and Farese, R.V. (1999). Insulin activates protein kinases C-ζ and C-λ by an autophosphorylation-dependent mechanism and stimulates their translocation to GLUT4 vesicles and other membrane fractions in rat adipocytes. *Journal of Biological Chemistry*, 274, 25308-25316.

Appendix A. STATE VARIABLES

The states mentioned in Fig. 1 and in the text are summarized in Tab. A.1. The states mentioned in Fig. 2, $X_1 - X_{11}$, refer to different configurations of insulin receptor, as explained in Kiselyov et al. [2009].

Table A.1. State variables description

State	Description
X_{12}	Unphosphorylated insulin receptor substrate-1, IRS1
X_{13}	Tyrosine-phosphorylated IRS1, IRS1-Yp
X_{14}	Unactivated phosphatidylinositol-3-kinase, PI3K
X_{15}	Activated IRS1-PI3K complex (M)
X_{16}	Phosphatidylinositol triphosphate, PI(3,4,5)P3
X_{17}	Phosphatidylinositol diphosphate, PI(4,5)P2
X_{18}	Phosphatidylinositol diphosphate, PI(3,4)P2
X_{19}	Unactivated protein kinase Akt
X_{20}	Activated Akt, Akt p
X_{21}	Unactivated protein kinase C, PKCζ
X_{22}	Activated PKCζ, PKCζp
X_{23}	Intracellular glucose transporter, GLUT4 cyt
X_{24}	Serine-phosphorylated IRS1, IRS1-Sp
X_{25}	Membrane GLUT4, GLUT4m

Appendix B. MODEL EQUATIONS

Model equations for the receptor compartment are listed in Tab. B.1. The names of the state variables are given in Fig. 2, and I represents insulin concentration.

$$
\begin{aligned}
\dot{X}_1 &= (-2(a_1+a_2)I - k_4)X_1 + d_1X_2 + d_2X_3 + k_{-4}X_{11} \\
\dot{X}_2 &= 2a_1IX_1 - (k_{cr} + (a_1+a_2)I + d_1 + k_4)X_2 + d_2X_4 \\
&\quad + d_2X_5 + 2d_1X_6 \\
\dot{X}_3 &= 2a_2IX_1 - (k_{cr} + (a_1+a_2)I + d_2 + k_4)X_3 + d_1X_4 \\
&\quad + d_1X_5 + 2d_2X_7 \\
\dot{X}_4 &= k_{cr}X_2 + k_{cr}X_3 - (d_1 + d_2 + (a_1+a_2)I + k_{4'})X_4 \\
&\quad + d_1X_8 + d_2X_9 \\
\dot{X}_5 &= a_2IX_2 + a_1IX_3 - (d_1 + d_2 + 2k_{cr} + k_4)X_5 \\
&\quad + d_1X_8 + d_2X_9 \\
\dot{X}_6 &= a_1IX_2 - (2(d_1 + k_{cr}) + k_4)X_6 + d_2X_8 \\
\dot{X}_7 &= a_2IX_3 - (2(d_2 + k_{cr}) + k_4)X_7 + d_1X_9 \\
\dot{X}_8 &= a_1IX_4 + k_{cr}X_5 + 2k_{cr}X_6 - (2d_1 + d_2 + a_2I \\
&\quad + k_{4'})X_8 + d_2X_{10} \\
\dot{X}_9 &= a_2IX_4 + k_{cr}X_5 + 2k_{cr}X_7 - (d_1 + 2d_2 + a_1I \\
&\quad + k_{4'})X_9 + d_1X_{10} \\
\dot{X}_{10} &= a_2IX_8 + a_1IX_9 - (d_1 + d_2 + k_{4'})X_{10} \\
\dot{X}_{11} &= k_4(X_1 + X_2 + X_3 + X_5 + X_6 + X_7) + k_{4'}(X_4 + X_8 \\
&\quad + X_9 + X_{10}) + -(k_{-4} + k_{-5})X_{11} + k_5
\end{aligned}
\tag{B.1}
$$

The model equations for the downstream reactions were taken from Sedaghat et al. [2002].

Appendix C. MODEL PARAMETERS

Parameters of the multiscale model are summarized in Tab. C.1, where parameters from Sedaghat et al. [2002] are also reported for reference.

With respect to Sedaghat et al. [2002], parameters k_5 and PTP were defined by means of the hyperbolic tangent function to avoid discontinuities, what negligibly affected model results:

$$
k_5 = k_{5,1}\tanh[-10^{15}(X_{11} - k_{5,3})] + k_{5,2} \tag{C.1}
$$

$$
\begin{aligned}
PTP = &(PTP_1X_{20} - PTP_2)\tanh[10^{15}(X_{20} - PTP_3)] \\
&+ (PTP_2 - PTP_1X_{20}).
\end{aligned}
\tag{C.2}
$$

State-dependent parameters from Sedaghat et al. [2002] were deconvolved as follows:

$$k_9 = k_{9,1}X_{15} + k_{9,2} \tag{C.3}$$

$$k_{11} = k_{11,1}X_{16} - k_{11,2} \tag{C.4}$$

$$k_{12} = k_{12,1}X_{16} - k_{12,2} \tag{C.5}$$

$$k_{13'} = k_{13',1}X_{20} + k_{13',2}X_{22}. \tag{C.6}$$

Table C.1. Model parameters

No	Parameter	Sedaghat [2002]	Multiscale model
1	k_1 $(s^{-1}M^{-1})$	10^6	-
2	k_{-1} (s^{-1})	$3.33 \cdot 10^{-3}$	-
3	k_2 $(s^{-1}M^{-1})$	10^6	-
4	k_{-2} (s^{-1})	$3.33 \cdot 10^{-1}$	-
5	k_3 (s^{-1})	41.67	-
6	k_{-3} $(s^{-1}M^{-1})$	$3.33 \cdot 10^{-3}$	-
7	k_{-4} (s^{-1})	$5 \cdot 10^{-5}$	$3.43 \cdot 10^{-5}$
8	k_4 (s^{-1})	$5.55 \cdot 10^{-6}$	$3.82 \cdot 10^{-6}$
9	$k_{4'}$ (s^{-1})	$3.5 \cdot 10^{-5}$	$4.88 \cdot 10^{-5}$
10	$k_{-4'}$ (s^{-1})	$3.5 \cdot 10^{-6}$	-
11	k_{-5} (s^{-1})	$2.78 \cdot 10^{-20}$	$3.04 \cdot 10^{-20}$
12	k_6 $(s^{-1}M^{-1})$	$7.68 \cdot 10^{-3}$	-
13	k_7/IR_p $(s^{-1}M^{-1})$	$7.73 \cdot 10^{10}$	$1.24 \cdot 10^{11}$
14	k_{-7} $(s^{-1}M^{-1})$	$2.33 \cdot 10^{-2}$	$3.72 \cdot 10^{-2}$
15	k_{-8} (s^{-1})	$1.67 \cdot 10^{-1}$	$8.60 \cdot 10^{-2}$
16	k_8 $(s^{-1}M^{-1})$	$1.18 \cdot 10^{10}$	$6.07 \cdot 10^{9}$
17	k_{-9} $(s^{-1}M^{-1})$	$7.02 \cdot 10^{-1}$	$7.45 \cdot 10^{-1}$
18	k_{-10} $(s^{-1}M^{-1})$	$4.62 \cdot 10^{-2}$	$7.88 \cdot 10^{-2}$
19	k_{10} (s^{-1})	$4.94 \cdot 10^{-2}$	$8.42 \cdot 10^{-2}$
20	k_{-11} (s^{-1})	$1.16 \cdot 10^{-1}$	$1.72 \cdot 10^{-3}$
21	k_{-12} (s^{-1})	$1.16 \cdot 10^{-1}$	$1.70 \cdot 10^{-1}$
22	k_{-13} (s^{-1})	$2.78 \cdot 10^{-3}$	$2.17 \cdot 10^{-3}$
23	k_{13} (s^{-1})	$1.16 \cdot 10^{-4}$	$9.04 \cdot 10^{-5}$
24	k_{-14} (s^{-1})	$1.93 \cdot 10^{-5}$	$2.11 \cdot 10^{-5}$
25	k_{14} (s^{-1})	$1.85 \cdot 10^{-3}$	$2.03 \cdot 10^{-3}$
26	$k_{7'}$ $(s^{-1}M^{-1})$	$5.78 \cdot 10^{-3}$	$4.07 \cdot 10^{-3}$
27	$k_{-7'}$ (s^{-1})	$1.43 \cdot 10^{-3}$	10^{-3}
28	V_{max}	20	20
29	K_d	12	12
30	n	4	4
31	$SHIP$ (M)	1	1
32	$PTEN$ (M)	1	1
33	$k_{5,1}$ (Ms^{-1})	$6.96 \cdot 10^{-19}$	$1.27 \cdot 10^{-20}$
34	$k_{5,2}$ (Ms^{-1})	$9.74 \cdot 10^{-19}$	$1.77 \cdot 10^{-20}$
35	$k_{5,3}$ (M)	10^{-13}	10^{-13}
36	$k_{9,1}$ (s^{-1})	$8.23 \cdot 10^{12}$	$8.73 \cdot 10^{12}$
37	$k_{9,2}$ (s^{-1})	$2.19 \cdot 10^{-3}$	$2.32 \cdot 10^{-3}$
38	$k_{11,1}$ (s^{-1})	$4.14 \cdot 10^{-3}$	$6.17 \cdot 10^{-5}$
39	$k_{11,2}$ (s^{-1})	$1.28 \cdot 10^{-3}$	$1.91 \cdot 10^{-5}$
40	$k_{12,1}$ (s^{-1})	$4.14 \cdot 10^{-3}$	$6.1 \cdot 10^{-3}$
41	$k_{12,2}$ (s^{-1})	$1.28 \cdot 10^{-3}$	$1.89 \cdot 10^{-3}$
42	$k_{13',1}$ (s^{-1})	$3.83 \cdot 10^{-5}$	$2.98 \cdot 10^{-5}$
43	$k_{13',2}$ (s^{-1})	$1.53 \cdot 10^{-4}$	$1.19 \cdot 10^{-4}$
44	PTP_1 (M)	$1.38 \cdot 10^{-2}$	$1.38 \cdot 10^{-2}$
45	PTP_2 (M)	0.5	0.5
46	PTP_3	36.36	36.36
47	a_1 $(s^{-1}M^{-1})$	-	$5.58 \cdot 10^{5}$
48	a_2 $(s^{-1}M^{-1})$	-	$3.69 \cdot 10^{5}$
49	d_1 (s^{-1})	-	$4.72 \cdot 10^{-3}$
50	d_2 (s^{-1})	-	$1.22 \cdot 10^{-2}$
51	k_{cr} (s^{-1})	-	$3.8 \cdot 10^{-3}$
52	τ (s)	90	90